The Rigid-Body Dynamics of a Single-Rotor, Two-Axis gimbaled Gyro Assembly for Line-of-Sight Stabilization

Riju Chatterjee

January 31, 2023

Contents

1 Context and Objective **2**
1.1 Optics 2

2 Modeling **2**
2.1 System Description 2
2.2 State Space and Forcing 5
2.3 Simplifying Assumptions 6
2.4 Rotation Matrices 7
2.5 Inertias 8

3 Lagrangian Formulation **9**

4 Linearized Model **9**
4.1 Resonance and Stability 10
4.2 Steady-State Response to Sinusoidal Excitation 11

5 Models of Second Order and Higher **13**

6 A Representative System Example **14**
6.1 Linearized Behavior 14
6.2 Damping 14
6.3 Non-Linear Effects 14

7 Ansys Simulations **17**

8 Conclusion **26**

1 Context and Objective

Line-of-sight stabilization is performed in some battle tanks by means of a single-rotor, two-axis gimbaled gyroscope that is mechanically coupled to a correcting mirror. The goal of this analysis is:

1. to derive governing equations for such an assembly,
2. to build a linear model of the system that can be used for contol system design,
3. to study the bounds of applicability of the linear model through numerical investigation of the magnitude of nonlinear effects, and
4. to find the effect of system parameters on LoS stabilization performance.

1.1 Optics

The nature of the gyro-mirror coupling required for line-of-sight correction is dictated by elementary considerations of the optics of reflections.

A change by angle θ in the orientation of the tank would cause a change of magnitude θ in the angle of incidence of a space-fixed ray of light onto a tank-fixed mirror. The angle of reflection would therefore also change by θ, and the net change in the direction relative to the tank of the reflected ray would be 2θ. As seen in Fig. 1, however, a change by angle $\frac{1}{2}\theta$ in the orientation of the mirror relative to the tank allows the direction relative to the tank of the reflected ray to be maintained unchanged. Rotation of the mirror by $\frac{1}{2}\theta$ can be achieved to the extent that the gyroscope maintains its orientation in space, by coupling the mirror to the gyroscope by a 2:1 reduction; this is in fact the mechanism employed in such LoS stabilization systems.

2 Modeling

The gyro assembly is modeled as a collection of rigid bodies with motion constraints relative to each other and to a moving base (the tank).

2.1 System Description

Figure 2 shows the tank and the components of the gyro assembly. The system as considered here consists of the tank, plus four rigid bodies. An inertial

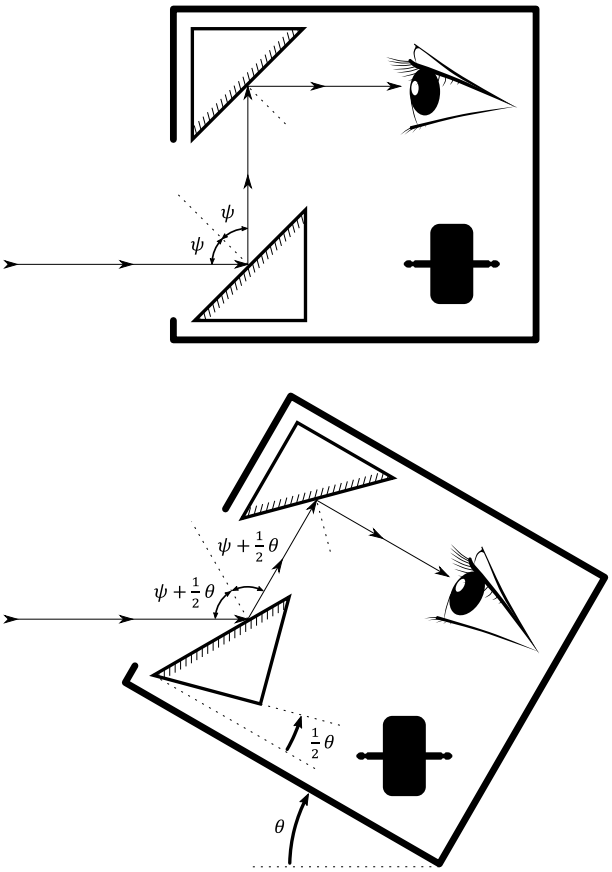

Figure 1: Optical ideal for LoS correction in 1D

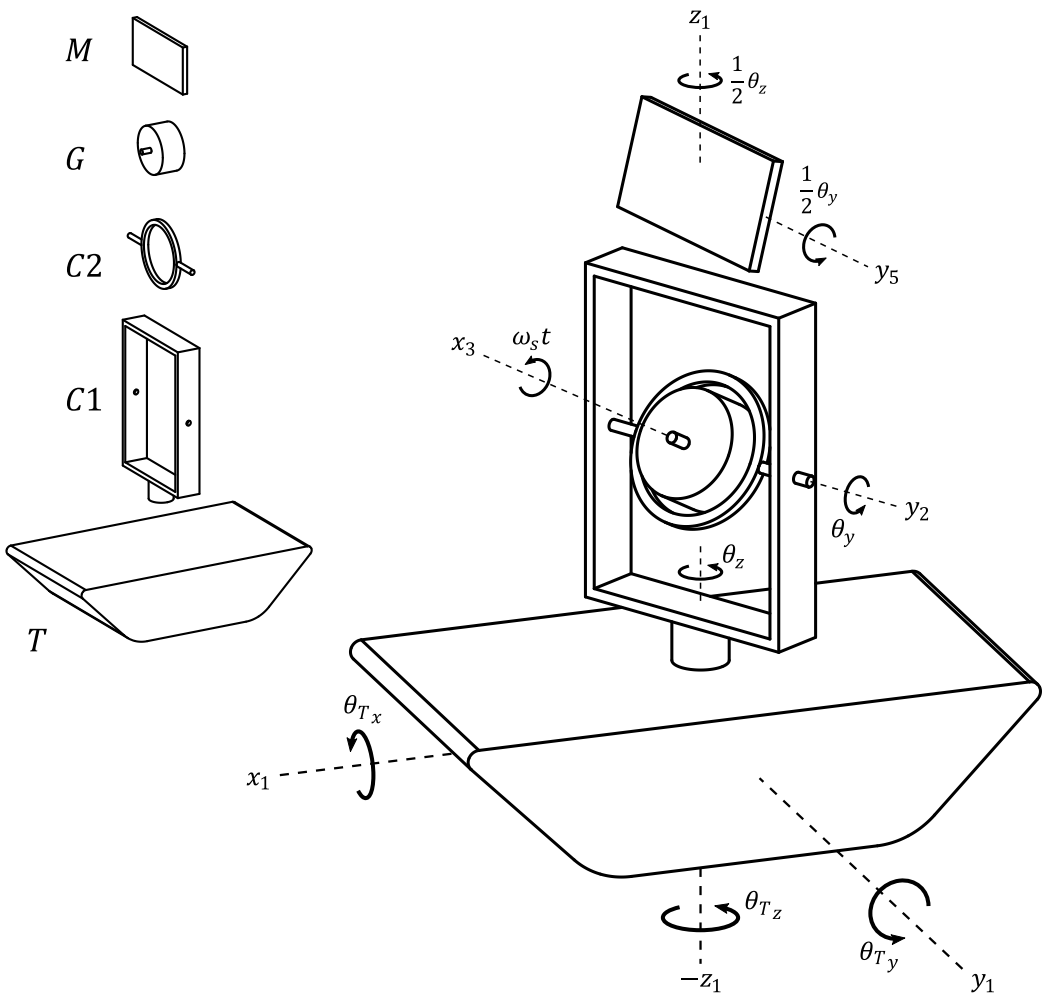

Figure 2: The gyro system

coordinate system $x_0y_0z_0$ and body-fixed coordinate systems originating at the center of mass of each body are chosen such that when the assembly is in its reference configuration, the x-axis is parallel to the gyro spin axis and the z-axis points vertically upward. The coordinate systems $x_1y_1z_1$, $x_2y_yz_2$, $x_3y_3z_3$, $x_4y_4z_4$, and $x_5y_5z_5$ are fixed, in order, to:

1. The tank T
2. The first chassis component C1, which is attached to the tank and at any time is additionally rotated about the tank-fixed z-axis z_1 by angle θ_z.
3. The second chassis component C2, which is attached to C1 and at any time is additionally rotated about the C1-fixed y-axis y_2 by angle θ_y.
4. The gyro rotor G, which is attached to C2 and additionaly spins about the C2-fixed x-axis x_3 at speed ω_s.
5. The correcting mirror M, which is attached to the tank and is additionally rotated about z_1 by $\frac{1}{2}\theta_z$ and about the body-fixed y-axis y_5 by $\frac{1}{2}\theta_y$.

2.2 State Space and Forcing

Dynamical models of mechanical systems often aim to characterize system response to imposed forces and moments. In the case of the gyro assembly, however, the performance of the system is measured by the gyroscope's ability to maintain its orientation in spite of the imposed motion of the tank. Any useful calculations using a force-and-moment based model would therefore pre-require the additional, fairly complicated calculation of the forces and moments corresponding to the tank's motion. It is most sensible, therefore, to bypass this intermediate step by considering the forcing to the gyro assembly to consist of the tank's orientation as a function of time. This is done by using time-variant x-y-z Euler angles θ_{Tx}, θ_{Ty} and θ_{Tz} to define the tank's orientation.

Given the values and the first and second time derivatives of θ_{Tx}, θ_{Ty} and θ_{Tz} at any time, the system state is defined completely by the values and the first and second time derivatives of θ_y and θ_z. θ_y and θ_z can therefore serve as generalized coordinates for the system. The reference configuration corresponds to $\theta_{Tx} = \theta_{Ty} = \theta_{Tz} = \theta_y = \theta_z = 0$ and time $t = 0$.

2.3 Simplifying Assumptions

The principal simplifying assumption made here is that the gyroscope gimbal is centered, balanced, and symmetric, as expected in a well-designed system. Balancing and centering have the effect that translational and rotational dynamics decouple, and calculations involving rotational motions and inertias can be performed without involving translations or the net mass of bodies. Due to symmetry, the principal axes of inertia of the gimbal components and of the gyro rotor can be assumed to be along the chosen body-fixed coordinate axes, resulting in diagonal matrix representations of moment-of inertia tensors and greatly simplifying any analytical expressions obtained.

The assumptions of centering, balancing, and symmetry are not only realistic, but also fairly robust. The effect of small imbalances in the mounting of the gimbal is largely that of additional rotational inertia as given by the parallel axis theorem, and the translational kinetic energy of a gyroscope is in general so much smaller than its rotational energy that translations can be expected to have a vanishingly small effect on system dynamics. The effects of moderate misalignment of gimbal components' principal axes of inertia is small as well, since their rotations are constrained to specific bearing axes and general precessive motions are not possible.

Since the precise nature of the gimbal-mirror coupling is unknown and it is expected to be a fairly lightweight mechanism, it has been ignored here except as the enforcer of a motion constraint. The nature of the constraint, moreover, is not precisely known, since it depends on the nature of the coupling. While the optical ideal is presumably for the orientation of the mirror to be given by half the effective rotation angle and the same effective rotation axis as the orientation of C2 is given by, the implementation of this constraint is mechanically difficult and analytically complicated. The constraint assumed in this analysis is therefore that of halved Euler angles. The correcting mirror itself is of unknown shape and size, and so has been assumed to have equal principal moments of inertia to simplify expressions obtained.

Lastly, no attempt is made in this analysis to include physically realistic dissipation, based on the assumption that the gyroscope gimbal bearings are well-lubricated and the effects of dissipation are small beyond the suppression of spin-induced oscillations (wobble), for which ad-hoc linear damping is used here.

2.4 Rotation Matrices

The orientation of T, C1, C2, G and M can be represented by rotation tensors R_T, R_{C1}, R_{C2}, R_G, and R_M, such that the rotation tensor corresponding to a body transforms any vector embedded in that body from its value in the assembly's reference configuration to its current value.

The orientation of the tank is defined by x-y-z Euler angles θ_{Tx}, θ_{Ty}, and θ_{Tz}, so R_T is given by

$$[R_T] = \begin{bmatrix} 1 & 0 & 0 \\ 0 & \cos\theta_{Tx} & -\sin\theta_{Tx} \\ 0 & \sin\theta_{Tx} & \cos\theta_{Tx} \end{bmatrix} \begin{bmatrix} \cos\theta_{Ty} & 0 & \sin\theta_{Ty} \\ 0 & 1 & 0 \\ -\sin\theta_{Ty} & 0 & \cos\theta_{Ty} \end{bmatrix} \begin{bmatrix} \cos\theta_{Tz} & -\sin\theta_{Tz} & 0 \\ \sin\theta_{Tz} & \cos\theta_{Tz} & 0 \\ 0 & 0 & 1 \end{bmatrix} \tag{1}$$

where square brackets without a subscript denote a component matrix in the inertial coordinate system $x_0y_0z_0$.

Since the gyro assembly is assumed to be balanced and centered, their centers of mass, which are the origins of their respective body-fixed coordinate systems, coincide. The rotations of C1, C2 and G about z_1, y_2 and x_3 are therefore exactly equivalent to rotations by the same angles about z_2, y_3 and x_4, and each of these rotations can therefore be expressed simply as a rotation about a body-fixed coordinate axis.

C1 rotates with T and undergoes an additional body-fixed z-axis rotation by θ_z, so R_{C1} is given by

$$[R_{C1}] = [R_T] \begin{bmatrix} \cos\theta_z & -\sin\theta_z & 0 \\ \sin\theta_z & \cos\theta_z & 0 \\ 0 & 0 & 1 \end{bmatrix} \tag{2}$$

C2 rotates with C1 and undergoes an additional body-fixed y-axis rotation by θ_y, so R_{C2} is given by

$$[R_{C2}] = [R_{C1}] \begin{bmatrix} \cos\theta_y & 0 & \sin\theta_y \\ 0 & 1 & 0 \\ -\sin\theta_y & 0 & \cos\theta_y \end{bmatrix} \tag{3}$$

G rotates with C2 and undergoes an additional body-fixed x-axis rotation by $\omega_s t$, so R_G is given by

$$[R_G] = [R_{C2}] \begin{bmatrix} 1 & 0 & 0 \\ 0 & \cos\omega_s t & -\sin\omega_s t \\ 0 & \sin\omega_s t & \cos\omega_s t \end{bmatrix} \tag{4}$$

M rotates with the tank and undergoes additional body-fixed z-axis and y-axis rotations by $\frac{1}{2}\theta_z$ and $\frac{1}{2}\theta_y$, assumed here to be in that order. R_M is therefore given by

$$[R_M] = [R_T] \begin{bmatrix} \cos\frac{1}{2}\theta_z & -\sin\frac{1}{2}\theta_z & 0 \\ \sin\frac{1}{2}\theta_z & \cos\frac{1}{2}\theta_z & 0 \\ 0 & 0 & 1 \end{bmatrix} \begin{bmatrix} \cos\frac{1}{2}\theta_y & 0 & \sin\frac{1}{2}\theta_y \\ 0 & 1 & 0 \\ -\sin\frac{1}{2}\theta_y & 0 & \cos\frac{1}{2}\theta_y \end{bmatrix} \tag{5}$$

2.5 Inertias

As discussed, the matrix representations in the chosen body-fixed coordinate systems of the moment of inertia tensors of the four rigid bodies considered in this analysis are expected to be diagonal. Separately, the mirror M is, as a simplification, assumed to have equal principal moments of inertia, and the gyro rotor itself has equal transverse moments of inertia due to axisymmetry. The inertias of the bodies in this analysis are therefore given by:

$$[I_{C1}]_{x_2y_2z_2} = \begin{bmatrix} I_{C1x} & 0 & 0 \\ 0 & I_{C1y} & 0 \\ 0 & 0 & I_{C1z} \end{bmatrix} \tag{6}$$

$$[I_{C2}]_{x_3y_3z_3} = \begin{bmatrix} I_{C2x} & 0 & 0 \\ 0 & I_{C2y} & 0 \\ 0 & 0 & I_{C3z} \end{bmatrix} \tag{7}$$

$$[I_G]_{x_4y_4z_4} = \begin{bmatrix} I_{Gax} & 0 & 0 \\ 0 & I_{Gtr} & 0 \\ 0 & 0 & I_{Gtr} \end{bmatrix} \tag{8}$$

$$[I_M]_{x_5y_5z_5} = \begin{bmatrix} I_m & 0 & 0 \\ 0 & I_m & 0 \\ 0 & 0 & I_m \end{bmatrix} \tag{9}$$

The matrix representation in space-fixed coordinates $x_0y_0z_0$ of the moment of inertia tensor of each body can be found using:

$$[I] = [R][I]_{x_ny_nz_n}[R]^T \tag{10}$$

where $[I]_{x_ny_nz_n}$ is the body-fixed moment of inertia matrix, $[I]$ is the space-fixed moment of inertia matrix, and R is the rotation defining the body's current orientation.

3 Lagrangian Formulation

This analysis is concerned primarily with the motions of the parts of the gyro assembly in response to the motion of the tank, and not particularly with the reactive forces and moments generated in the course of these motions. The methods of Lagrangian mechanics are therefore particularly suitable here, since they allow the implicit incorporation of motion constraints. As discussed earlier, θ_y and θ_z are a natural choice of generalized coordinates for the system.

Since the gyro assembly contains no springs, masses undergoing net vertical motion, or other sources of potential energy, the Lagrangian is equal simply to the net kinetic energy of the system, given by:

$$L = \sum E_k = \frac{1}{2}\vec{\omega}_{C1} \cdot I_{C1}\vec{\omega}_{C1} + \frac{1}{2}\vec{\omega}_{C2} \cdot I_{C2}\vec{\omega}_{C2} + \frac{1}{2}\vec{\omega}_G \cdot I_G\vec{\omega}_G + \frac{1}{2}\vec{\omega}_M \cdot I_M\vec{\omega}_M \quad (11)$$

where the angular velocity of each body can be found as the axial vector of $R\dot{R}^T$, i.e.,

$$[\vec{\omega}] = \begin{bmatrix} [\dot{R}R^T]_{3,2} \\ [\dot{R}R^T]_{1,3} \\ [\dot{R}R^T]_{2,1} \end{bmatrix} \quad (12)$$

where R is the rotation defining the orientation of the body.

Lagrange's equations can therefore be written for the system:

$$\frac{d}{dt}\frac{\partial L}{\partial \dot{\theta}_y} - \frac{\partial L}{\partial \theta_y} = 0 \quad (13)$$

$$\frac{d}{dt}\frac{\partial L}{\partial \dot{\theta}_z} - \frac{\partial L}{\partial \theta_z} = 0 \quad (14)$$

4 Linearized Model

A linear small-deflection model of the behavior of the gyro assembly can be obtained by approximating L from (11) by a Taylor expansion upto second order about $\theta_{Tx} = \theta_{Ty} = \theta_{Tz} = \theta_y = \theta_z = 0$. This leads to (13) and (14) becoming linear due to the once-differentiation of L with respect to θ_y and θ_z and their rates of change. Solving these two, now linear, equations for $\ddot{\theta}_y$ and $\ddot{\theta}_z$ gives:

$$\ddot{\theta}_y = -\frac{2\left(2I_{C2y} + 2I_{Gtr} + I_m\right)\ddot{\theta}_{Ty} + 4I_{Gax}\omega_s\left(\dot{\theta}_z + \dot{\theta}_{Tz}\right)}{4I_{C2y} + 4I_{Gtr} + I_m} \quad (15)$$

and

$$\ddot{\theta}_z = -\frac{2\left(2I_{C1z} + 2I_{C2z} + 2I_{Gtr} + I_m\right)\ddot{\theta}_{Tz} - 4I_{Gax}\omega_s\left(\dot{\theta}_y + \dot{\theta}_{Ty}\right)}{4I_{C1z} + 4I_{C2z} + 4I_{Gtr} + I_m} \tag{16}$$

Alternately, new variables $\theta_{erry} = \theta_y + \theta_{Ty}$ and $\theta_{errz} = \theta_z + \theta_{Tz}$ representing the error in LoS correction can be substituted into the linearized governing equations to replace θ_y and θ_z. This results in

$$\ddot{\theta}_{erry} = -\frac{I_m\ddot{\theta}_{Ty} + 4I_{Gax}\omega_s\dot{\theta}_{errz}}{4I_{C2y} + 4I_{Gtr} + I_m} \tag{17}$$

and

$$\ddot{\theta}_{errz} = -\frac{I_m\ddot{\theta}_{Tz} - 4I_{Gax}\omega_s\dot{\theta}_{erry}}{4I_{C1z} + 4I_{C2z} + 4I_{Gtr} + I_m} \tag{18}$$

It is interesting to note that the *only* forcing-dependent terms in (17) and (18) are scaled by I_m. It may be reasonably asserted, therefore, that any model of the system that does not incorporate mirror inertia is fundamentally incapable of accurately predicting the system response to forcing.

4.1 Resonance and Stability

Substituting $\ddot{\theta}_{Ty} = \ddot{\theta}_{Tz} = 0$ into (17) and (18) give the linearized governing equations for the unforced motion of the gyro system, which can then be written in first-order form as

$$\begin{bmatrix} \dot{\theta}_{erry} \\ \dot{\theta}_{errz} \\ \ddot{\theta}_{erry} \\ \ddot{\theta}_{errz} \end{bmatrix} = H \begin{bmatrix} \theta_{erry} \\ \theta_{errz} \\ \dot{\theta}_{erry} \\ \dot{\theta}_{errz} \end{bmatrix} \tag{19}$$

where

$$H = \begin{bmatrix} 0 & 0 & 1 & 0 \\ 0 & 0 & 0 & 1 \\ 0 & 0 & 0 & -\dfrac{4I_{Gax}\omega_s}{4I_{C2y} + 4I_{Gtr} + I_m} \\ 0 & 0 & \dfrac{4I_{Gax}\omega_s}{4I_{C1z} + 4I_{C2z} + 4I_{Gtr} + I_m} & 0 \end{bmatrix} \tag{20}$$

The eigenvalues of H are:

$$\begin{gathered} 0, \\ 0, \\ -\frac{4I_{Gax}\omega_s}{\sqrt{-\left(4I_{C2y}+4I_{Gtr}+I_m\right)\left(4I_{C1z}+4I_{C2z}+4I_{Gtr}+I_m\right)}}, \\ \frac{4I_{Gax}\omega_s}{\sqrt{-\left(4I_{C2y}+4I_{Gtr}+I_m\right)\left(4I_{C1z}+4I_{C2z}+4I_{Gtr}+I_m\right)}} \end{gathered}$$

Clearly, the only nonzero eigenvalues are a single conjugate pair of imaginary numbers. This means that the system is marginally stable and has one natural frequency, which is given by the magnitude of the imaginary eigenvalues:

$$\omega_n = \frac{4I_{Gax}\omega_s}{\sqrt{\left(4I_{C2y}+4I_{Gtr}+I_m\right)\left(4I_{C1z}+4I_{C2z}+4I_{Gtr}+I_m\right)}} \tag{21}$$

4.2 Steady-State Response to Sinusoidal Excitation

Specifying the excitation to the gyro system as time-variant Euler angles can be interpreted physically as the system being mounted on an external gimbal with actuators in the joints, as shown in Fig. 3. Considering the simple sinusoidal exitation

$$\theta_{Ty} = \theta_{Tz} = A_1 \sin \omega_{ex} t \tag{22}$$

and assuming a general sinusoidal response

$$\theta_{erry} = A_2 \sin \omega_{ex} t + B_2 \cos \omega_{ex} t \tag{23}$$

$$\theta_{errz} = A_3 \sin \omega_{ex} t + B_3 \cos \omega_{ex} t \tag{24}$$

A_2, B_2, A_3, and B_3 can be solved for in terms of A_1 and ω_{ex} from the system of equations formed by substituting (22) through (24) into (17) and (18). The amplitudes of the responses in the y and z-directions, i.e., in pitch and in yaw, can then be calculated as $\theta_{erry_{\max}} = \sqrt{A_2^2 + B_2^2}$ and $\theta_{errz_{\max}} = \sqrt{A_3^2 + B_3^2}$, giving

$$\theta_{erry_{\max}} = \frac{A_1 I_m \omega_{ex} \sqrt{\omega_{ex}^2 \left(4I_{C1z}+4I_{C2z}+4I_{Gtr}+I_m\right)^2 + 16 I_{G_{ax}}^2 \omega_s^2}}{\omega_{ex}^2 \left(4I_{C2y}+4I_{Gtr}+I_m\right)\left(4I_{C1z}+4I_{C2z}+4I_{Gtr}+I_m\right) - 16 I_{G_{ax}}^2 \omega_s^2} \tag{25}$$

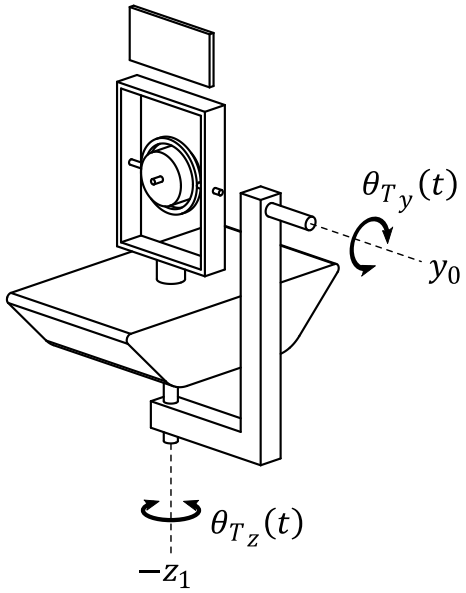

Figure 3: The physical interpretation of excitation via Euler angles

and

$$\theta_{err_{z\max}} = \frac{A_1 I_m \omega_{ex} \sqrt{\omega_{ex}^2 \left(4I_{C2_y} + 4I_{Gtr} + I_m\right)^2 + 16 I_{G_{ax}}^2 \omega_s^2}}{\omega_{ex}^2 \left(4I_{C2_y} + 4I_{Gtr} + I_m\right)\left(4I_{C1_z} + 4I_{C2_z} + 4I_{Gtr} + I_m\right) - 16 I_{G_{ax}}^2 \omega_s^2} \tag{26}$$

The phase lead of the responses in the y and z-directions are given by $\phi_{err_y} = \tan^{-1}\frac{B_2}{A_2}$ and $\phi_{err_z} = \tan^{-1}\frac{B_3}{A_3}$, which simplify to

$$\phi_{err_y} = \tan^{-1}\left(\frac{\omega_s 4 I_{Gax}}{\omega_{ex}\left(4I_{C1_z} + 4I_{C2_z} + 4I_{Gtr} + I_m\right)}\right) \tag{27}$$

and

$$\phi_{err_z} = -\tan^{-1}\left(\frac{\omega_s 4 I_{Gax}}{\omega_{ex}\left(4I_{C2_y} + 4I_{Gtr} + I_m\right)}\right) \tag{28}$$

As expected, (25) and (26) indicate that the system response is scaled by I_m for sinusoidal forcing (already known from (17) and (18) to be more generally true) and predict infinite amplitude as ω_{ex} approaches ω_n from (21).

5 Models of Second Order and Higher

While a linearized model is analytically convenient, it provides only a local approximation to system behaviour. Models incorporating higher-order effects can be generated by changing the point of truncation of the Taylor expansion of the system Lagrangian, and the Lagrangian can be used without approximation to obtain an exact model.

Using a third-order approximation to L, for example, results in the following second-order model of system behavior:

$$\begin{aligned}\ddot{\theta}_{erry} =& \frac{1}{4I_{C2y} + 4I_{Gtr} + I_m}\Big(4I_{C2y}\theta_{errz}\ddot{\theta}_{Tx} - 4I_{Gax}\dot{\theta}_{errz}\omega_s - I_m\ddot{\theta}_{Ty} \\ & - 4I_{C2x}\dot{\theta}_{errz}\dot{\theta}_{Tx} + 4I_{C2y}\dot{\theta}_{errz}\dot{\theta}_{Tx} + 4I_{C2z}\dot{\theta}_{errz}\dot{\theta}_{Tx} - 4I_{Gax}\dot{\theta}_{errz}\dot{\theta}_{Tx} \\ & + 4I_{Gtr}\theta_{errz}\ddot{\theta}_{Tx} + 8I_{Gtr}\dot{\theta}_{errz}\dot{\theta}_{Tx} + I_m\theta_{errz}\ddot{\theta}_{Tx} + I_m\dot{\theta}_{errz}\dot{\theta}_{Tx} \\ & + I_m\ddot{\theta}_{Tx}\theta_{Tz} + I_m\dot{\theta}_{Tx}\dot{\theta}_{Tz} - 4I_{Gax}\theta_{erry}\omega_s\dot{\theta}_{Tx}\Big)\end{aligned} \tag{29}$$

$$\begin{aligned}\ddot{\theta}_{errz} =& \frac{1}{4I_{C1z} + 4I_{C2z} + 4I_{Gtr} + I_m}\Big(4I_{Gax}\dot{\theta}_{erry}\omega_s - I_m\ddot{\theta}_{Tz} + 4I_{C2x}\theta_{erry}\ddot{\theta}_{Tx} \\ & - 4I_{C2z}\theta_{erry}\ddot{\theta}_{Tx} + 4I_{C2x}\dot{\theta}_{erry}\dot{\theta}_{Tx} - 4I_{C2y}\dot{\theta}_{erry}\dot{\theta}_{Tx} - 4I_{C2z}\dot{\theta}_{erry}\dot{\theta}_{Tx} \\ & + 4I_{Gax}\theta_{erry}\ddot{\theta}_{Tx} + 4I_{Gax}\dot{\theta}_{erry}\dot{\theta}_{Tx} - 4I_{Gtr}\theta_{erry}\ddot{\theta}_{Tx} - 8I_{Gtr}\dot{\theta}_{erry}\dot{\theta}_{Tx} \\ & - I_m\dot{\theta}_{erry}\dot{\theta}_{Tx} - 4I_{C2x}\theta_{Ty}\ddot{\theta}_{Tx} - 4I_{C1z}\theta_{Ty}\ddot{\theta}_{Tx} + 4I_{C1x}\dot{\theta}_{Tx}\dot{\theta}_{Ty} \\ & - 4I_{C1y}\dot{\theta}_{Tx}\dot{\theta}_{Ty} - 4I_{C1z}\dot{\theta}_{Tx}\dot{\theta}_{Ty} - 4I_{Gax}\theta_{Ty}\ddot{\theta}_{Tx} - 2I_m\theta_{Ty}\ddot{\theta}_{Tx} \\ & - I_m\dot{\theta}_{Tx}\dot{\theta}_{Ty} - 4I_{Gax}\theta_{errz}\omega_s\dot{\theta}_{Tx}\Big)\end{aligned} \tag{30}$$

Such higher-order models are of little use beyond for numerical simulations, since nonlinear differential equations do not generally have analytical solutions. Nonlinear models can, however, help illuminate the nature of the limitations of the linearized model. Here, for example, (29) and (30) show that tank roll (θ_{Tx} and its time-derivatives) has an effect on LoS stabilization performance that is not captured by (17) and (18).

6 A Representative System Example

The following representative inertia values are now considered:

$$\begin{aligned} I_{C1x} = I_{C1y} = I_{C1z} &= 0.001\text{Kgm}^2 \\ I_{C2x} = I_{C2y} = I_{C2z} &= 0.0001\text{Kgm}^2 \\ I_{Gax} &= 0.0004\text{Kgm}^2 \\ I_{Gtr} &= 0.0001\text{Kgm}^2 \\ I_m &= 0.0001\text{Kgm}^2 \end{aligned}$$

allowing some numerical investigation of the behavior of the gyro system.

6.1 Linearized Behavior

Relative error in LoS correction in pitch and yaw can be calculated by dividing $\theta_{err_{y_{\max}}}$ and $\theta_{err_{z\max}}$ from (25) and (26) by A_1 and the net error can be estimated by dividing $\sqrt{\theta_{err_{y_{\max}}}^2 + \theta_{err_{z\max}}^2}$ by $\sqrt{2}A_1$. Fig. 4 shows the frequency response of the system considered here, with a gyro spin speed of 3000 rad/s.

The natural frequency of the system as predicted by (21) is 2285.71 rad/s, or around 364 Hz. There is, of course, an obvious peak seen at this frequency in Fig. 4.

6.2 Damping

Numerical solution of the system's governing equations with small nonzero initial conditions shows oscillatory behavior at the natural frequency. Introducing some ad-hoc damping into the equations causes these oscillations to die down. High levels of damping negatively affect LoS stabilization.

Figs. 5, 6 and 7 show examples of the undamped, morderately damped, and heavily damped behavior of the system.

6.3 Non-Linear Effects

This section presents simulations (i.e., numerical solutions of governing equations with prescribed forcing and initial conditions) using the linearized model from (17) and (18) and using nonlinear models like discussed in Section 5. Comparison between such simulations provides insight into the bounds of applicability of the linearized model.

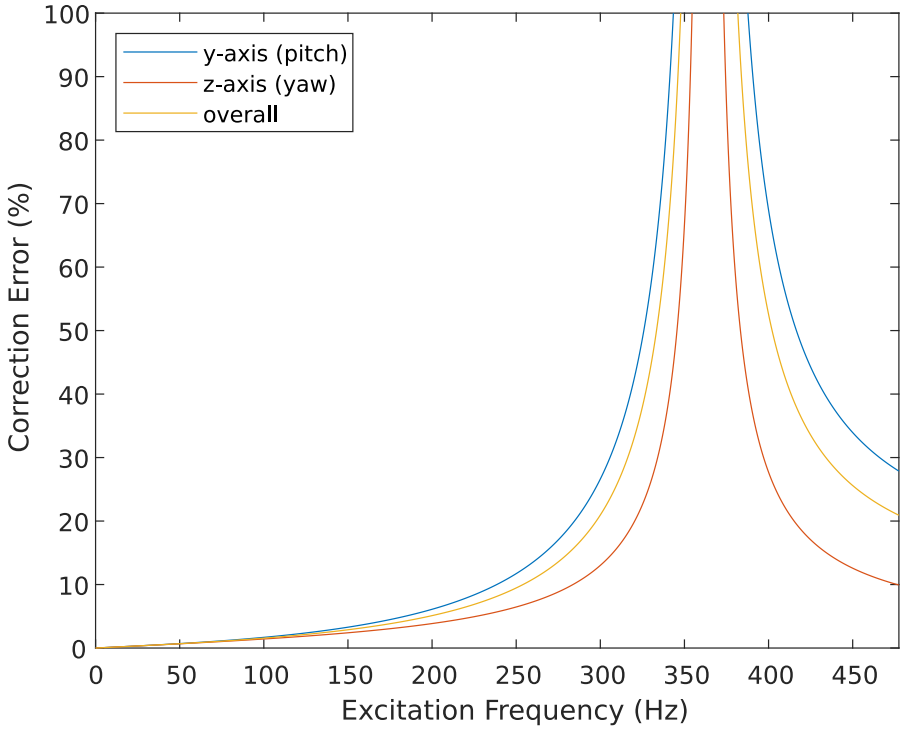

Figure 4: Frequency response of representative gyro system

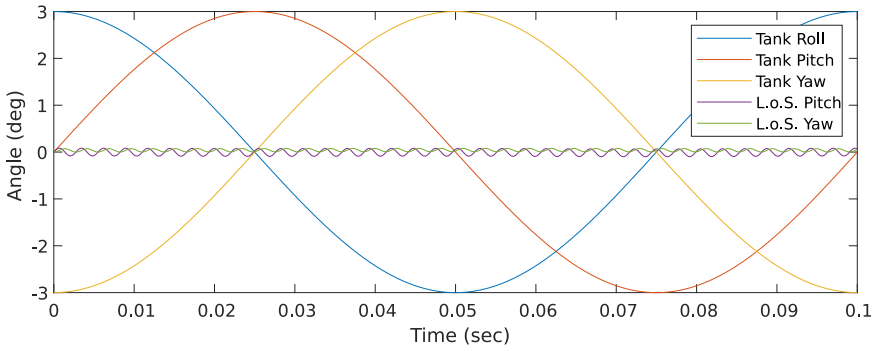

Figure 5: Undamped response

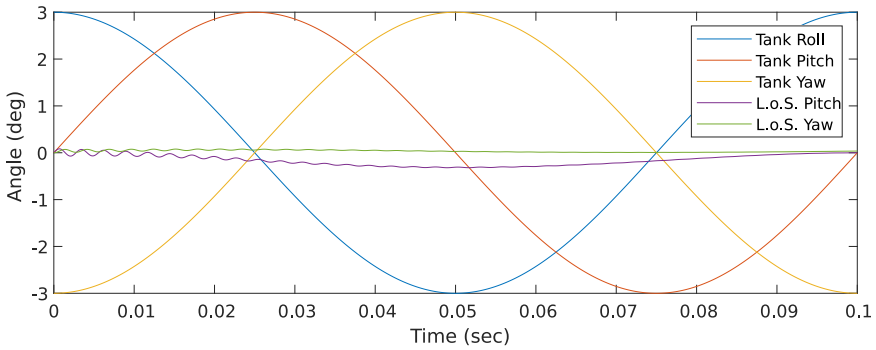

Figure 6: Moderately damped response

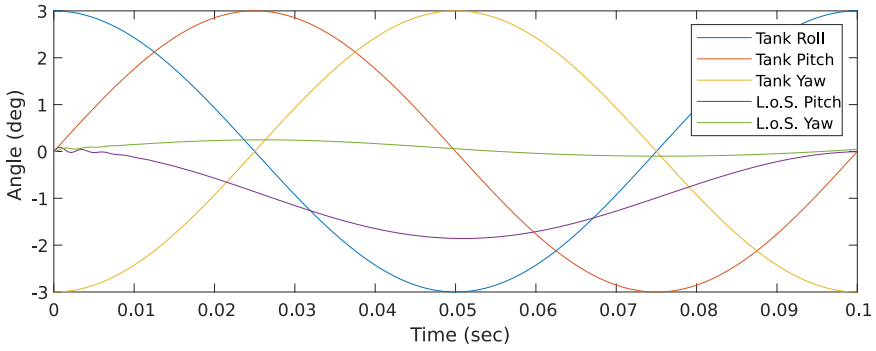

Figure 7: Heavily damped response

6.3.1 Second-Order Effect

As discussed in Section 5, an interesting behavior captured by a second-order model of the system and not captured by the linear model is the effect of tank roll. In any system configuration except the reference configuration, the gyro spin axis is not perfectly aligned with the tank roll axis. Tank roll therefore forces change in spin axis of the gyro and affects the system response.

Figs. 8, 9, and 10 show the response of the system as predicted by linear, second-order and full non-linear models to excitation in roll only. Nonzero initial conditions are used, since misalignment of the gyro axis is required for the effect of roll to manifest. The linear model predicts no deflection of the LoS from the initial configuration, but the second-order and full non-linear models agree in prediction of a significant deflection.

6.3.2 Third-Order Effect

A third-order model captures the effect of amplitude fairly well, where the first and second-order models do not. Figs. 11 through 16 show the response of the system as predicted by models of different orders to low and high amplitude excitation. The linear model works very well for excitations with an amplitude of 5°(greater than most realistic deflections of interest). With an excitation amplitude of 44°, however, the linear and second-order models under-predict the LoS deflection, while the predictions of the third-order model are close to those of the full non-linear model.

7 Ansys Simulations

The Rigid Body Dynamics module in Ansys allows imposition of constraint equations relating, among other things, rates of rotation in revolute joints. This feature makes it fairly straightforward to incorporate the 2:1 reduction considered here into a rigid body model of the system like seen in Fig. 17. Excitation can be introduced using an external gimbal, as illustrated in Fig. 3.

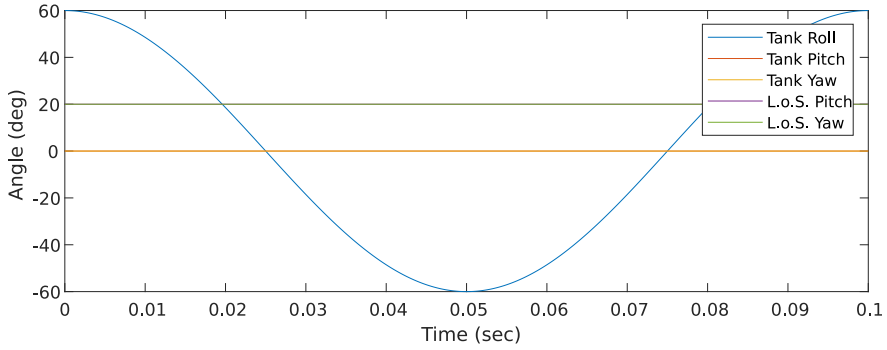

Figure 8: Linear response to tank roll

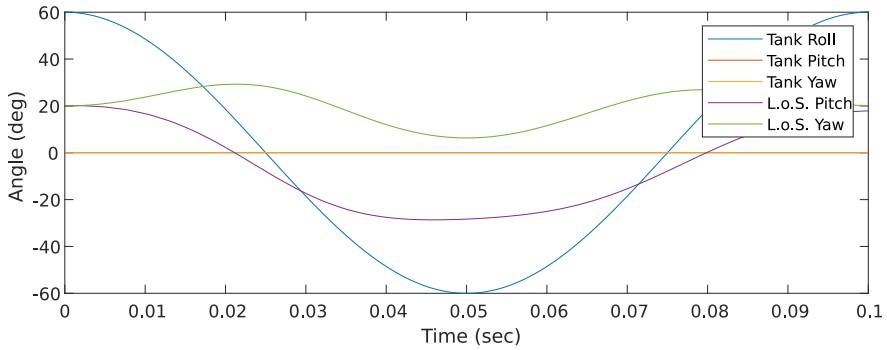

Figure 9: Second-order response to tank roll

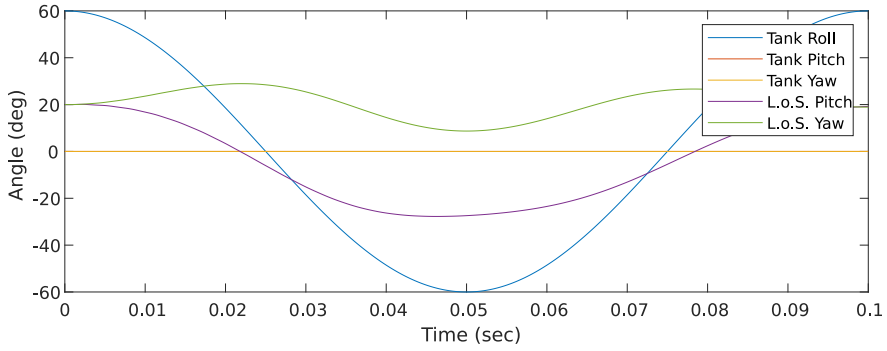

Figure 10: Full non-linear response to tank roll

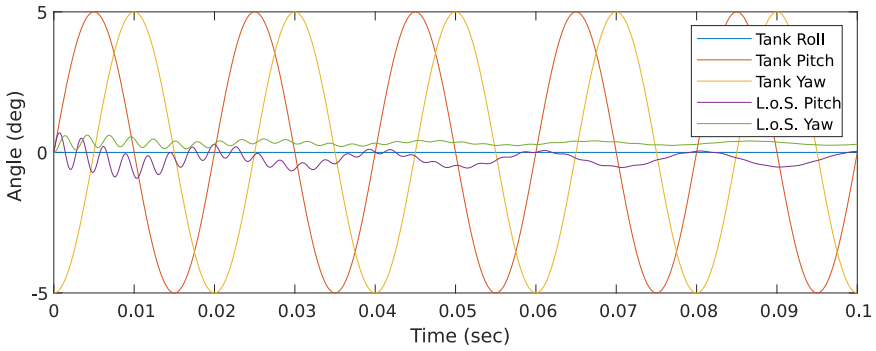

Figure 11: Linear response to low-amplitude excitation

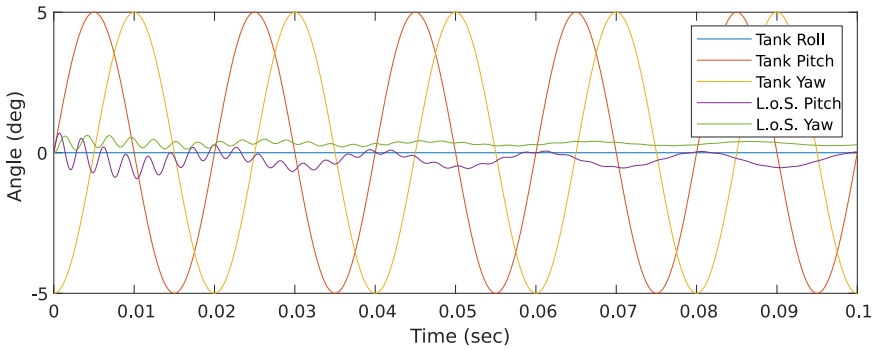

Figure 12: Full non-linear response to low-amplitude excitation

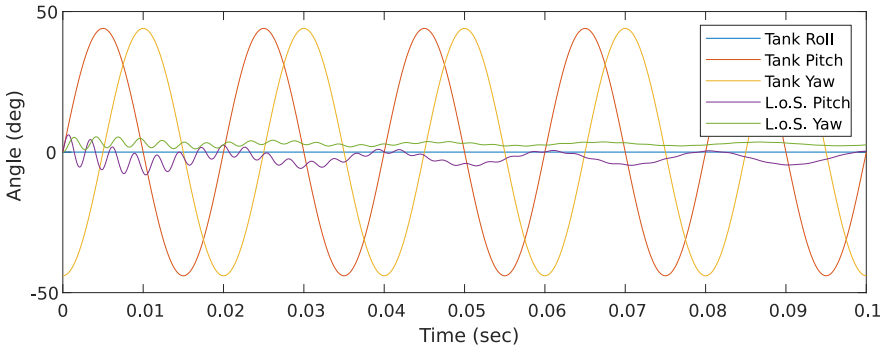

Figure 13: Linear response to high-amplitude excitation

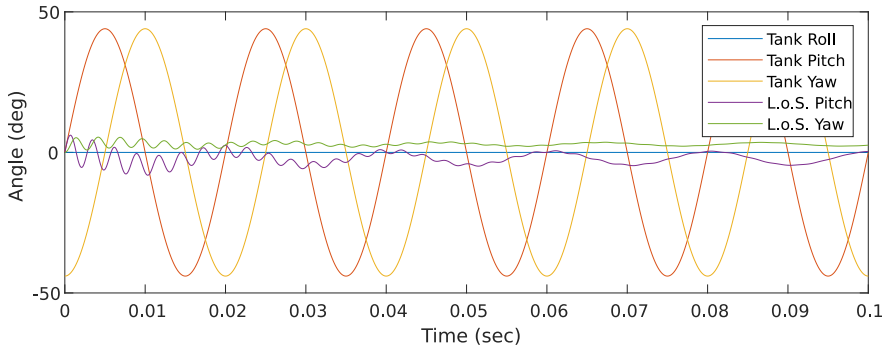

Figure 14: Second-order response to high-amplitude excitation

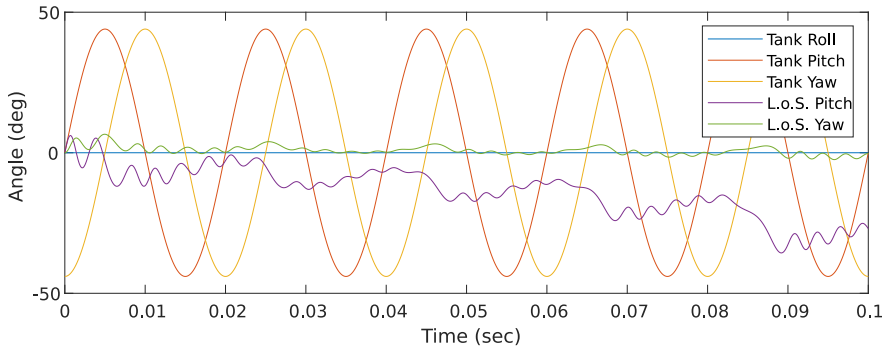

Figure 15: Third-order response to high-amplitude excitation

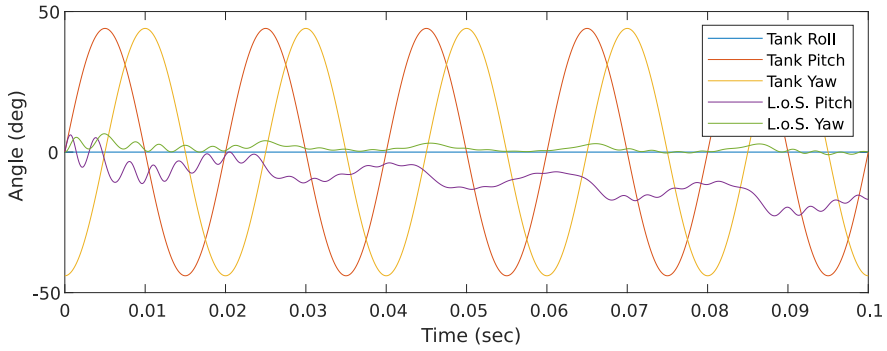

Figure 16: Full non-linear response to high-amplitude excitation

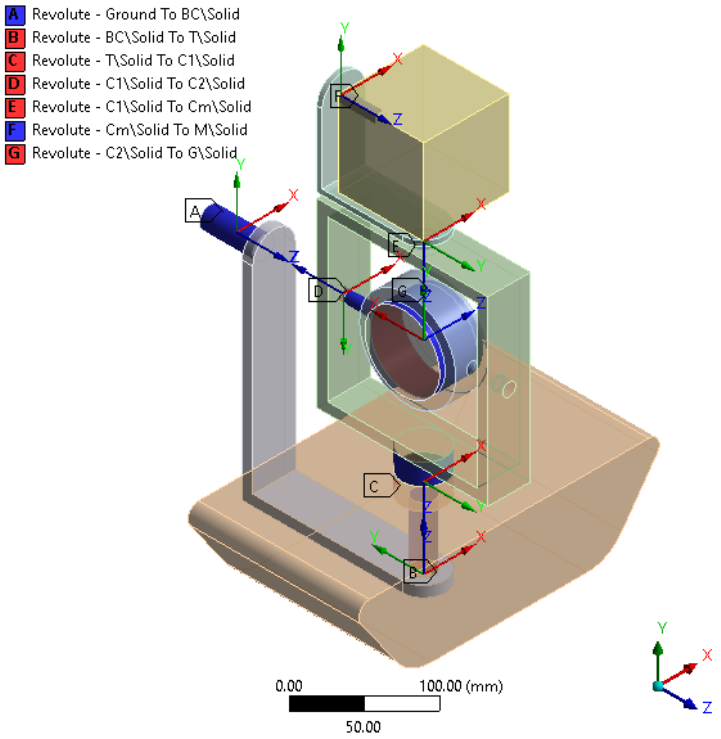

Figure 17: Rigid Body Dynamics simulation setup in Ansys

Ansys reported the following inertia values for the example system used:

$$
\begin{aligned}
I_{C1x} &= 0.009904\text{Kgm}^2 \\
I_{C1y} &= 0.007663\text{Kgm}^2 \\
I_{C1z} &= 0.001701\text{Kgm}^2 \\
I_{C2x} &= 0.001064\text{Kgm}^2 \\
I_{C2y} &= 0.000628\text{Kgm}^2 \\
I_{C2z} &= 0.000525\text{Kgm}^2 \\
I_{Gax} &= 0.000738\text{Kgm}^2 \\
I_{Gtr} &= 0.000530\text{Kgm}^2 \\
I_{m} &= 0.001666\text{Kgm}^2
\end{aligned}
$$

Numerical solutions of the derived governing equations using these inertia values, a spin speed of 3000 rad/s, and sinusoidal excitation of various frequencies and amplitudes are shown in Figs. 18, 20 and 22. Figs. 19, 21 and 23 show plots of data generated in Ansys simulations for the same conditions. The gyro system has no preferred configuration. Some gradual drift is expected, therefore, and initial conditions can be expected to have a significant influence on the mean value of the response but not necessarily on the nature of fluctuations about that mean. It is natural, then, for the system response predicted by different simulations that might use different numerical integration schemes to differ by constant or slowly changing offsets. Ignoring such offsets, however, the behaviour predicted by Ansys and using the simplified governing equations derived here are in good agreement.

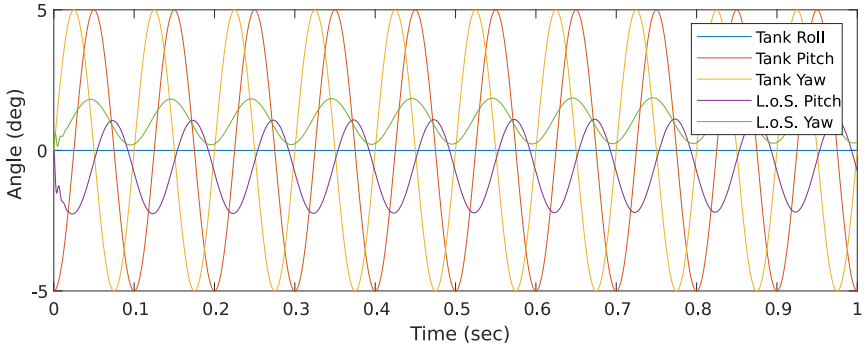

Figure 18: Simulation using derived governing equations: low amplitude excitation

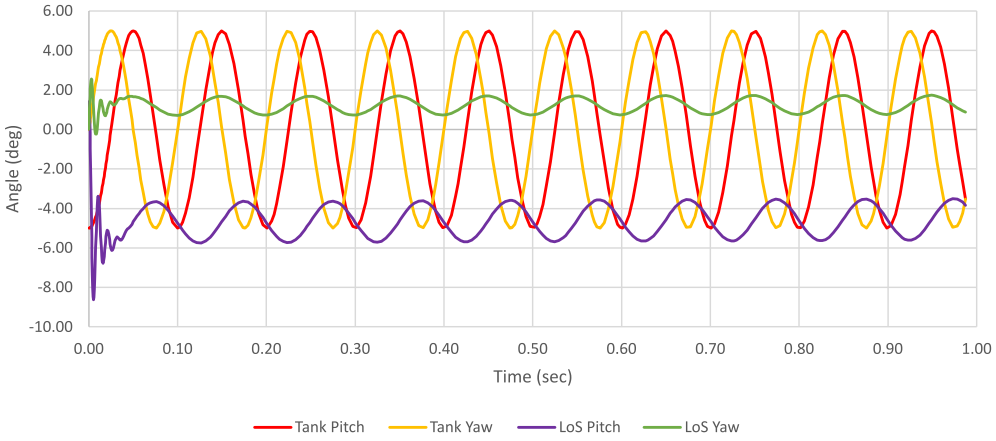

Figure 19: Ansys simulation: low amplitude excitation

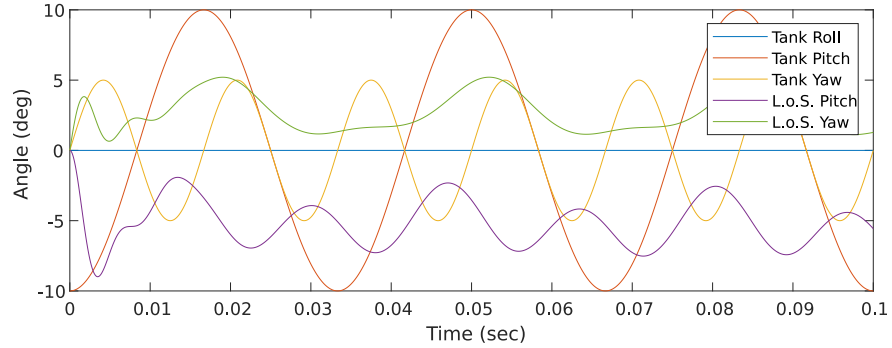

Figure 20: Simulation using derived governing equations: medium amplitude excitation

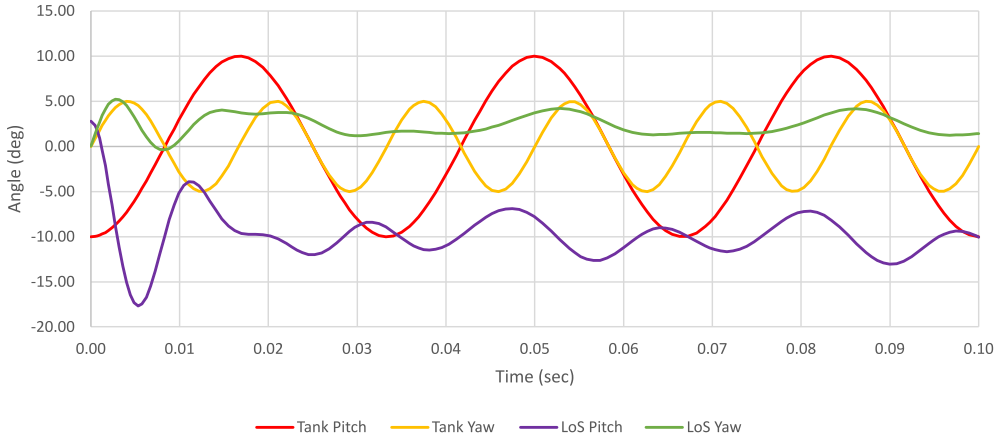

Figure 21: Ansys simulation: medium amplitude excitation

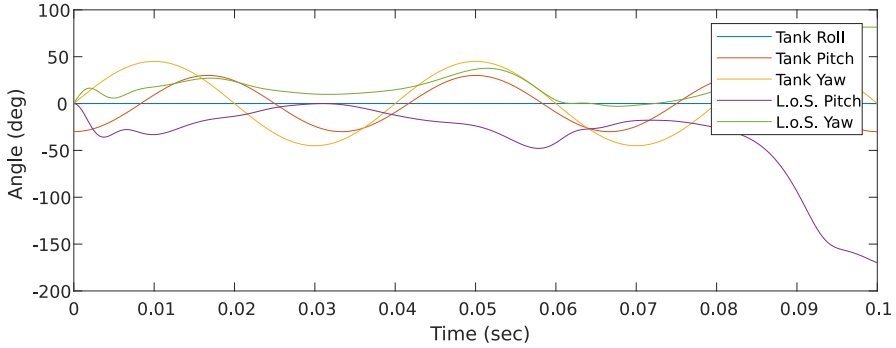

Figure 22: Simulation using derived governing equations: high amplitude excitation

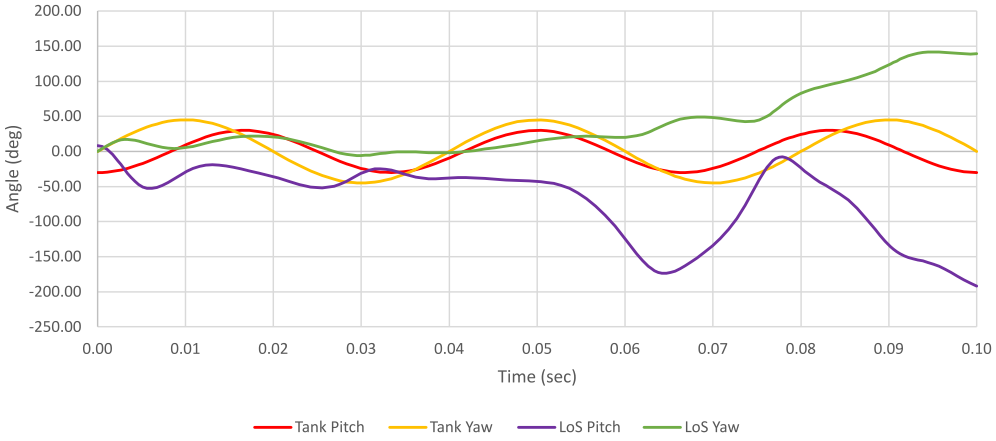

Figure 23: Ansys simulation: high amplitude excitation

8 Conclusion

This work has derived governing equations for a gyroscope on a two-axis gimbal coupled via a 2:1 reduction to a mirror for optical line-of-sight stabilization. Numerical solutions of these equations agree with results of Ansys simulations, showing that the derivation is correct. In a linearized model of system behavior, *the entire* dependence of response on forcing has been found to be scaled by the inertia of the mirror; this kind of system is therefore fundamentally different from free-gimbaled gyroscopes, and analytical results for free gyroscopes are not directly applicable.

The system has been found to be marginally stable at the nominal operating point and to have one resonant frequency. Expressions have been derived for this resonant frequency and for the amplitude and phase of the steady-state system response to sinusoidal excitation.

A second-order effect on stabilization performance of excitation about the nominal gyro axis has been identified, and the nonlinear effect of excitation amplitude has been found to be of third order. For one representative system example, the linearized model has been found to be reasonably accurate for excitation amplitudes of at least up to 5°.